Featured in Physics

Similarities and differences between nickelate and cuprate films grown on a SrTiO₃ substrate

Yang Zhang [1,2] Ling-Fang Lin [1,2] Wenjun Hu,[1] Adriana Moreo [1,3] Shuai Dong,[2] and Elbio Dagotto[1,3]

[1]*Department of Physics and Astronomy, University of Tennessee, Knoxville, Tennessee 37996, USA*
[2]*School of Physics, Southeast University, Nanjing 211189, China*
[3]*Materials Science and Technology Division, Oak Ridge National Laboratory, Oak Ridge, Tennessee 37831, USA*

The recent discovery of superconductivity in Sr-doped NdNiO₂ films grown on SrTiO₃ started a novel field within unconventional superconductivity. To understand the similarities and differences between nickelate and cuprate layers on the same SrTiO₃ substrate, here based on the density functional theory we have systematically investigated the structural, electronic, and magnetic properties of NdNiO₂/SrTiO₃ and CaCuO₂/SrTiO₃ systems. Our results revealed a strong lattice reconstruction in the case of NdNiO₂/SrTiO₃, resulting in a polar film, with the surface and interfacial NiO₂ layers presenting opposite displacements. To avoid the "polar catastrophe," the NiO₂ surface to the vacuum reconstructs as well. However, for CaCuO₂/SrTiO₃, the distortions of those same two CuO₂ layers were in the same direction. In addition, we found this distortion to be approximately independent of the studied range of film thickness for the nickelate films. Furthermore, we also observed a two-dimensional electron gas at the interface between NdNiO₂ and SrTiO₃, caused by the polar discontinuity, in agreement with recent literature. For NdNiO₂/SrTiO₃ the two-dimensional electron gas extends over several layers, while for CaCuO₂/SrTiO₃ this electronic rearrangement is very localized at the interface between CaCuO₂ and SrTiO₃. The electronic reconstruction found at the interface involves a strong occupation of the Ti $3d_{xy}$ state. In both cases, there is a significant electronic charge transfer from the surface Ni or Cu layers to the Ti interface layer. The interfacial Ni and Cu layers are hole and electron doped, respectively. By introducing magnetism and electronic correlation, we observed that the $d_{3z^2-r^2}$ orbital of Ni becomes itinerant while the same orbital for Cu remains doubly occupied, establishing a clear two- vs one-orbital active framework for the description of these systems. Furthermore, we also observed a strong magnetic reconstruction at the NdNiO₂ surface to vacuum layer where magnetism is basically suppressed.

I. INTRODUCTION

Since the discovery of superconductivity in the cuprates [1], two-dimensional (2D) correlated systems with transition-metal square lattice structures became the focus of research to study unconventional superconductors and potentially to continue increasing the critical temperature [2–5]. For this reason, the recent discovery of superconductivity in the infinite-layer Sr-doped NdNiO₂ (NNO) attracted much attention [6–10]. The discovery was reported employing films of NNO grown on SrTiO₃ (STO) [6], with a critical temperature $T_c \sim 15$ K. NNO displays a typical quasi-two-dimensional square lattice structure with the space group $P4/mmm$ (No. 123) [6], similar to the Cu-based CaCuO₂ (CCO) [11]. Since the $3d$ electronic occupied configuration of Ni^{1+} (d^9) is isoelectronic with Cu^{2+} (d^9), the superconducting mechanism of infinite-layer nickelate was expected to be similar to CCO, where superconductivity was found upon hole doping [11]. Many theoretical efforts revealed similarities and differences between individual infinite-layer nickelate and cuprates in bulk form [8,12–19].

However, recent developments indicate that superconductivity is absent in bulk Sr-doped NNO [20,21]. These results suggest that the existence of an NNO/STO interface may

be crucial to understand the superconductivity observed in the infinite-layer nickelate film. Moreover, superconductivity was also reported at the interface between CCO and STO [22,23]. This is all reminiscent of previous results for the LaAlO₃(LAO)/STO interface, where superconductivity was observed experimentally and attributed to an interfacial two-dimensional electron gas (2DEG) driven by the polar discontinuity [24–26]. Related STO perovskite interfaces have also been widely studied theoretically, leading to interesting predictions at those interfaces [27,28]. In addition, there are many efforts to engineer charge transfer and orbital polarization in LaTiO₃/LaNiO₃ superlattices to obtain superconductivity [29–31]. In this superlattice structure, due to carrier doping, a single $3d_{x^2-y^2}$ orbital was obtained at band edges, providing a general method for designing new superconductors.

It is surprising that a conducting system would emerge at the interface of two wide-gap insulating oxides [32,33]. In the LAO/STO system, it was found that the 2DEG would become magnetic and superconducting at low temperatures [25,34]. One possible explanation relies on the polar catastrophe that forces an interfacial reconstruction [33,35]. Furthermore, in the LAO/STO interface, the Ti $3d_{xy}$ orbital plays an important role for the interface ferromagnetism (FM) and supercon-

ductivity produced by such electronic reconstruction [36,37]. These interesting developments in LAO/STO interfaces, and the absence of superconductivity in bulk NNO, provides the framework for the present work, as well as recent efforts by other groups. Can a similar interesting interfacial phenomenon be crucial for the physics of NNO/STO interfaces? In particular, do nickelate and cuprate films display similar or different behavior when grown on a STO substrate?

In the infinite-layer nickelate, the system alternatively stacks the highly charged $(Nd)^{3+}$ and $(NiO_2)^{3-}$ layers along the [001] direction, while the STO substrate contains charge-neutral layers $(SrO)^0$ and $(TiO_2)^0$. This configuration would produce a net electric field inside the nickelate component, resulting from an electric potential that diverges as the NNO thickness grows. To avoid this "polar catastrophe," an electronic reconstruction occurs and hole doping [from Ni^{1+} (d^9) to Ni^{2+} (d^8)] at the interface could be expected, leading to an oscillating electric potential that remains finite. The possibility of "polar catastrophe" physics in the NNO/STO heterojunction was recently theoretically discussed in Ref. [38].

To better understand the similarities and differences between nickelate and cuprate films grown on an STO substrate, here using density functional theory (DFT) we provide a comprehensive first-principles study of NNO/STO and CCO/STO systems. Our main results are as follows: First, we found a strong lattice reconstruction in NNO/STO systems resulting in a polar nickelate film, with the limiting surface and interfacial NiO_2 layers presenting opposite displacements. On the other hand, in CCO/STO systems the distortions of those same two CuO_2 layers were in the same direction. Within our accuracy, the atomic reconstruction was basically independent of the thickness of the NNO films. Second, we also observed a strong electronic reconstruction for the two systems. Remarkably, and in agreement with our qualitative expectation, a 2DEG develops at the interfacial layer between NNO and STO due to the polar discontinuity. This electron gas extends over several layers beyond the interface. In CCO/STO systems, however, the electronic rearrangement was far more constrained in size and only observed at the interface between CCO and STO. The hole doping at the interfacial NiO_2 layer was observed, but the interfacial CuO_2 layer was found to be electron doped. By comparing the unrelaxed and relaxed slab models, we believe that the 2DEG was indeed induced by the polar discontinuity. Furthermore, a strong occupation of the Ti $3d_{xy}$ orbital was observed at the TiO_2 interface for both NNO/STO and CCO/STO systems. At the interfacial TiO_2 layer, the Ti $3d_{xy}$ orbital becomes occupied due to its energy being lowered by ~ -0.58 eV at the Γ point. In the $LaAlO_3/SrTiO_3$ interface, the Ti $3d_{xy}$ orbital is important for the observed interfacial FM and superconductivity [36,37]. Thus, it is reasonable to assume the strongly occupied Ti $3d_{xy}$ orbital may be associated to the observed superconductivity of the infinite-layer nickelates as well. By introducing magnetism in the calculations, the $d_{3z^2-r^2}$ orbital of Ni becomes itinerant, probably contributing to the nonmagnetic properties of the NNO/STO interface, while the $d_{3z^2-r^2}$ orbital of Cu remains doubly occupied and thus not relevant at the dopings considered experimentally, establishing another qualitative difference between the two cases. In addition, the

magnetism of the $NdNiO_2$ surface layer was basically suppressed.

II. METHOD AND MODEL SYSTEM

In contrast to the insulator cuprates, NNO displays metallic characteristics [6]. Studying the superconducting dome of $(Nd,Sr)NiO_2$, only a weakly insulating behavior was reported on both sides of the dome [9]. STO is a wideband semiconductor. To simulate the infinite-layer nickelates and cuprates grown on STO [001], we constructed the slab models using $(NNO)_n/(STO)_4$ and $(CCO)_n/(STO)_4$ superlattices ($n = 1$–8 are the layers of nickelate or cuprate films specifically analyzed here, corresponding to one to eight unit cells). To match the STO [001] substrate, the in-plane lattice constants were fixed as $a = b = 3.905$ Å, the STO values. Here, a 1×1 lattice in the xy plane was adopted without considering the octahedral rotations. These rotations could affect the STO bandwidth and should have an influence on the precise amount of charge transfer. However, those rotations will not change the tendency towards charge transfer since this is caused by the polar catastrophe. Furthermore, the octahedral rotations almost disappear at the TiO_2 interfacial layer [39]. Hence, to save computing resources, we have not introduced octahedral rotations since we focused on the qualitative phenomenon of charge transfer rather than on precise values of what amount of charge is transferred.

In the present study, we perform first-principles DFT calculations using the projector augmented wave (PAW) pseudopotentials with the Perdew-Burke-Ernzerhof (PBE) format, as implemented in the Vienna *Ab initio* Simulation Package (VASP) code [40–43]. We fixed the atomic positions of two STO layers to their bulk values [see Fig. 1(a)] while all other inner atomic positions were fully relaxed until the Hellman-Feynman force on each atom was smaller than 0.01 eV/Å. The plane-wave cutoff energy was 550 eV and the Nd $4f$ electrons are considered frozen in the core [7]. The mesh was appropriately modified for both the nonmagnetic (NM) and magnetic calculations to render the k-point densities approximately the same in reciprocal space (i.e., $15 \times 15 \times 1$ for the NM configuration).

Before studying heterostructures, we checked the physical properties of individual NNO, CCO, and STO, respectively [44]. Based on our structural optimization calculation with the PBE potential, the optimized crystal lattices of NNO are $a = b = 3.907$ Å and $c = 3.304$ Å, which are closed to the experimental bulk values ($a = b = 3.921$ Å and $c = 3.281$ Å) [6]. We also obtained the lateral lattice constants of STO ($a = b = 3.943$ Å) that are also in agreement with experimental values ($a = b = 3.905$ Å) [46]. Moreover, the optimized crystal lattices of CCO were found to be $a = b = 3.874$ Å and $c = 3.205$ Å, in good agreement with the corresponding bulk values ($a = b = 3.855$ Å and $c = 3.181$ Å) [11].

Then, we also calculated their electronic structures and found them to be consistent with previous calculations [7,8,14,18]. The detailed results of bulk electronic structures can be found in Appendix A. Furthermore, STO is known to be located at the vicinity between paraelectric and ferroelectric phases, rendering it sensitive to artificial strain. By fixing the crystal lattice of STO ($a = b = 3.905$ Å), then the
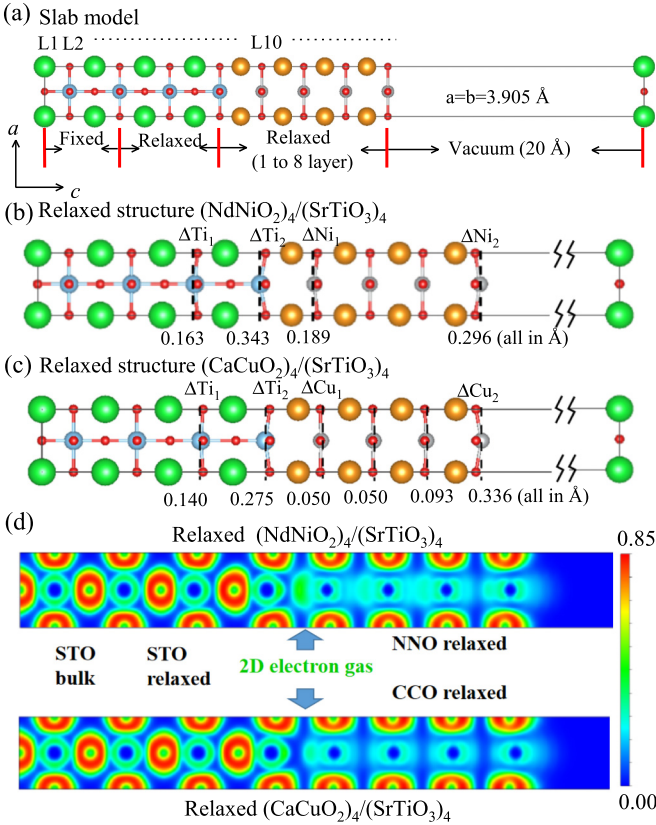
FIG. 1. (a) Schematic unrelaxed slab model of $(NNO)_n/(STO)_4$ with the following convention: orange, Nd or Ca; gray, Ni or Cu; red, O; green, Sr; blue, Ti. Here, we fixed $a = b = 3.905$ Å. We considered two undistorted STO layers (namely, with atomic positions fixed) to simulate the effects of the rest of the STO substrate. Schematic relaxed slab model of (b) $(NNO)_4/(STO)_4$ and (c) $(CCO)_4/(STO)_4$. (d) Electron localization function of the relaxed superlattice for $(NNO)_4/(STO)_4$ and $(CCO)_4/(STO)_4$.

relaxation procedure produced a value $c = 4.032$ Å that may lead to an artificial distortion because STO wishes to expand its lattice along the c axis. To verify this point, we also fixed the in-plane lattice to the optimized STO constants ($a = b = 3.943$ Å) and we found this procedure does not change the main conclusions (see Appendix B).

III. RESULTS

A. Atomic reconstruction

As illustrated in Fig. 1(b) for $n = 4$, both the surface and interfacial NiO$_2$ layers bend after structural relaxation, and the corresponding Ni ions move towards *different* directions with displacements $\Delta = 0.296$ and -0.189 Å. However, because the displacements are different in magnitude the net result is a polar film. The displacements of the Ni ions for the two central NiO$_2$ layers are much smaller. Furthermore, the interfacial Ti ions of the STO substrate show ferroelectric-like displacements away from the NNO/STO interface with values $\Delta = -0.343$ and -0.163 Å, respectively. Note that STO is known to be located at the vicinity between paraelectric and ferroelectric phases. Thus, the polar displacements of Ti may be affected by the ferroelectric distortion of STO itself

(this issue deserves further investigation beyond the scope of this publication). For the CCO/STO system, the Ti atoms also display similar ferroelectric-like distortions with similar displacements $\Delta = -0.275$ and -0.140 Å. However, the optimized CCO/STO superlattice indicates that the distortions of each CuO$_2$ layer are in the *same* direction along the c axis, as shown in Fig. 1(c). This results in a polar film as well. Polar distortions similar to those of CCO/STO systems observed here were also reported for LAO layers grown on STO [001] [47].

Those atomic displacements are relevant within the so-called polar catastrophe. When growing the highly charged $(Nd)^{3+}$ and $(NiO_2)^{3-}$ layers on the charge-neutral STO substrate, it will induce an ever-increasing dipole strength as the number of layers grows if the ionic charges are maintained at its normal value. In this case, a huge linear electrostatic potential across the NNO layers will cause the so-called polar catastrophe, as shown in Fig. 2(a). To avoid this phenomenon, the surfaces are expected to be reconstructed [see Fig. 2(a)]. In particular, an electronic reconstruction from Ni^{1+} (d^9) to Ni^{2+} (d^8) could be expected at the surface. As a result, the surface-vacuum polar distortion is induced by the polar field caused by the charge transfer. Namely, the lattice distortion is driven by the polar nature of the surface.

To better understand the effect of the film thickness for NNO and CCO, we fully relaxed the slab model using different numbers of NNO and CCO layers ($n = 1$–8, corresponding to one to eight unit cells). We observed that the distortion of the atomic layer reaches a value that is approximately independent of the film thickness for NNO/STO systems, at least within the range we studied. For CCO/STO systems, the distortion at the interfacial CuO$_2$ gradually reduces its value with increasing the film thickness. Moreover, as shown in Figs. 2(b) and 2(d), we observed that the thickness of the NNO and CCO layers does not alter the main qualitative results: (1) the two relaxed TiO$_2$ layers present a uniform polar distortion direction along the c axis both for NNO and CCO, and (2) the displacements of the surface and interfacial NiO$_2$ layers are opposite to each other, while the distortions of the surface and interfacial CuO$_2$ layers are in the same direction. In addition, the values of the displacements do not change substantially by increasing the film thickness of the NNO and CCO layers. We summarized the main displacements along the c axis in Figs. 2(b) and 2(d). Note the prominent difference between NNO and CCO with regard to the negative ΔNi_1 vs the positive ΔCu_1.

Furthermore, we also calculated the $3d$ electronic density for both $(NNO)_n/(STO)_4$ and $(CCO)_n/(STO)_4$ superlattices and compared with the corresponding bulk systems [see Figs. 2(b) and 2(d)]. For $(NNO)_n/(STO)_4$, by comparing with the bulk, it is clear that the relaxed two Ti sites gathered additional electrons while the surface Ni sites lost electrons, indicating the transfer of charge from the Ni surface to the interface with STO. Based on the DFT results [48], we estimate that for the case $n = 4$ the Ni surface lost charge by an amount -0.101 e/Ni, while the interface Ti gained about $+0.114$ e/Ti.

As described in the next paragraph in more detail, even the interfacial Ni loses electrons. We reach all these conclusions by comparing with the $3d$ electronic occupation in bulk
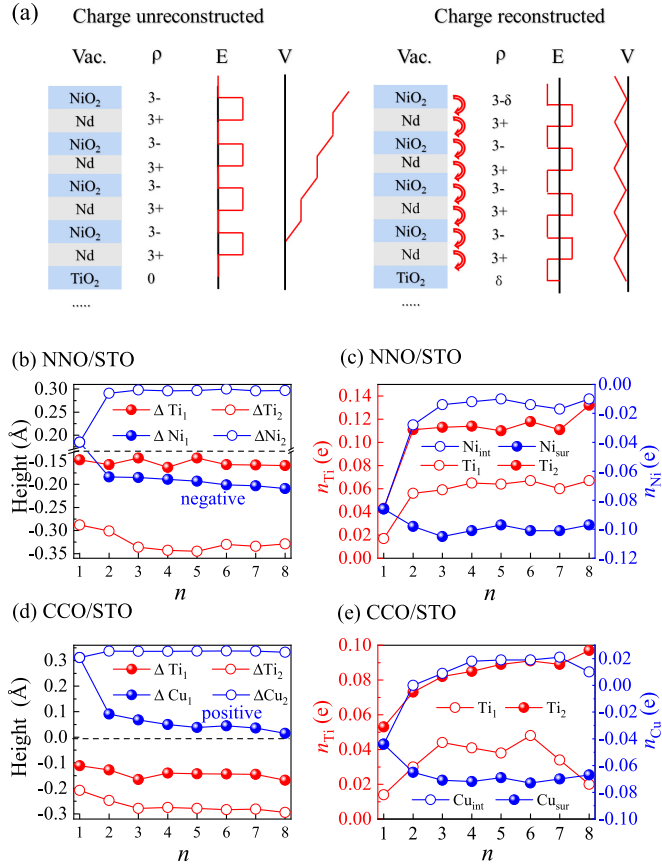
FIG. 2. (a) Possible polar catastrophe illustration predicted for $(NdNiO_2)_n/SrTiO_3$. (b) The displacements along the c axis for the four layers of Ni or Ti atoms corresponding to different superlattices $(NNO)_n/STO$ ($n = 1$–8). In Fig. 1(a) the notation ΔM ($M = Ni_1$, Ni_2, Cu_1, Cu_2, Ti_1, and Ti_2) was introduced. (c) The charge transfer of Ni and Ti atoms for different $(NNO)_n/(STO)_4$ ($n = 1$–8), compared with the corresponding bulk values. (d) The main displacements along the c axis for Cu or Ti atoms for different $(CCO)_n/(STO)_4$ ($n = 1$–8). (e) The charge transfer of Ni and Ti sites for different $(CCO)_n/(STO)_4$ ($n = 1$–8), compared with corresponding bulk values. In (c) and (e) the subscript "int" ("sur") denotes interface (surface). Note that the single MO_2 ($M = Ni$ or Cu) layer is both interface and surface for the $n = 1$ case.

NNO, in qualitative agreement with other recent theoretical calculations [39]. It should also be noted that this charge transfer behavior was also observed in the unrelaxed slab structure, indicating that the charge transfer is caused by the polar discontinuity; namely, it is electronic in origin, not due to the lattice relaxation. Due to the polar discontinuity, an intrinsic electronic reconstruction was also observed at the STO/LAO interface [33]. To avoid such polar catastrophe, the charge transfer occurred from surface to interface, leading to the observed conductivity [35] and superconductivity [34].

For the $(CCO)_n/(STO)_4$ superlattices, we also observed a hole-doping effect at the CuO_2 surface layer similar to the electrons transferred to the Ti interface for the case NNO/STO [see Fig. 2(e)]. The magnitude of charge transfer is slightly smaller for CCO than in the $(NNO)_n/(STO)_4$ system: here the surface Cu loses electrons with a net change

-0.072 e/Cu while the interface Ti attracts electrons with a net gain $+0.085$ e/Ti.

More specifically, let us quantitatively discuss the charge transfer at the Ni or Cu sites of each layer corresponding to the four-unit-cell NiO_2 or CuO_2 layers, with respect to their bulk properties. For the case of NNO/STO systems, all Ni sites (and corresponding layers) lose electrons. Because electrons are lost, we use a negative sign in front. From surface to interface, the lost electrons at each Ni are -0.101, -0.023, -0.005, and -0.012 e/Ni, respectively. This tendency towards charge transfer is also qualitatively consistent with previous generalized gradient approximation (GGA) $+ U$ calculations [39]. Both the electronic and atomic structures will affect the charge transfer in oxide interfaces [49,50]. In fact, we found that the Hubbard U on Ni sites would increase the charge transfer from the Ni surface, as discussed in Appendix C. Thus, all Ni layers lose electrons and those electrons move to the STO portion of the superlattice, primarily to the STO interfacial layer.

With respect to CCO/STO systems, the modifications in the number of electrons at the Cu sites from surface to interface are -0.072, -0.018, $+0.004$, and $+0.018$ e/Cu, respectively. The plus sign in the last two means that in the case of CCO the layers close to the interface gain electrons, the opposite behavior as for the case of NNO. In summary, for NNO the surface-Ni/interfacial-Ni/interfacial-Ti system displays hole/hole/electron doping, while for CCO the surface-Cu/interfacial-Cu/interfacial-Ti system displays hole/electron/electron doping. This different behavior may be due to the different bending bond direction of the interfacial NiO_2 and CuO_2 layers. The common factor is that in both cases the surface layer loses electrons that eventually are transferred in part to the Ti atoms. This behavior is similar to that reported in the LAO/STO system [36,37,51,52].

B. Electronic reconstruction

To study the movement of electrons due to the interface and generation of a 2D electron gas [53], we calculated the electron localization function (ELF) for both NNO/STO and CCO/STO interfaces [54], a quantity widely used within *ab initio* methods to characterize the electronic charge distribution. As shown in Fig. 1(d), there are extra electrons emerging at the NNO/STO interface leading to 2DEG characteristics. In addition, the electronic distribution located at the intermediate NiO_2 layers—between interface and surface—resembles the NNO/STO interface; namely, the 2DEG extends deep into the NNO region. For the CCO/STO system, we also observed the presence of extra electrons at the CCO/STO interface, but the rest of the CCO layers are not much affected.

As shown in Fig. 3(a), for the case without lattice reconstruction, the active O $2p$ orbitals shift closer to the Fermi level. This suggests that unoccupied oxygen $2p$ states may be involved in the electronic gas at the NiO_2 surface layer, supporting the p-d hybridization picture (namely, oxygen is not so deep in energy that it decouples). The STO layers far from the interface display band insulator behavior consistent with bulk STO. However, at the two STO layers near NNO, the Ti $3d$ orbital becomes partially occupied, resulting in metallic STO layers. Our DOS results clearly show
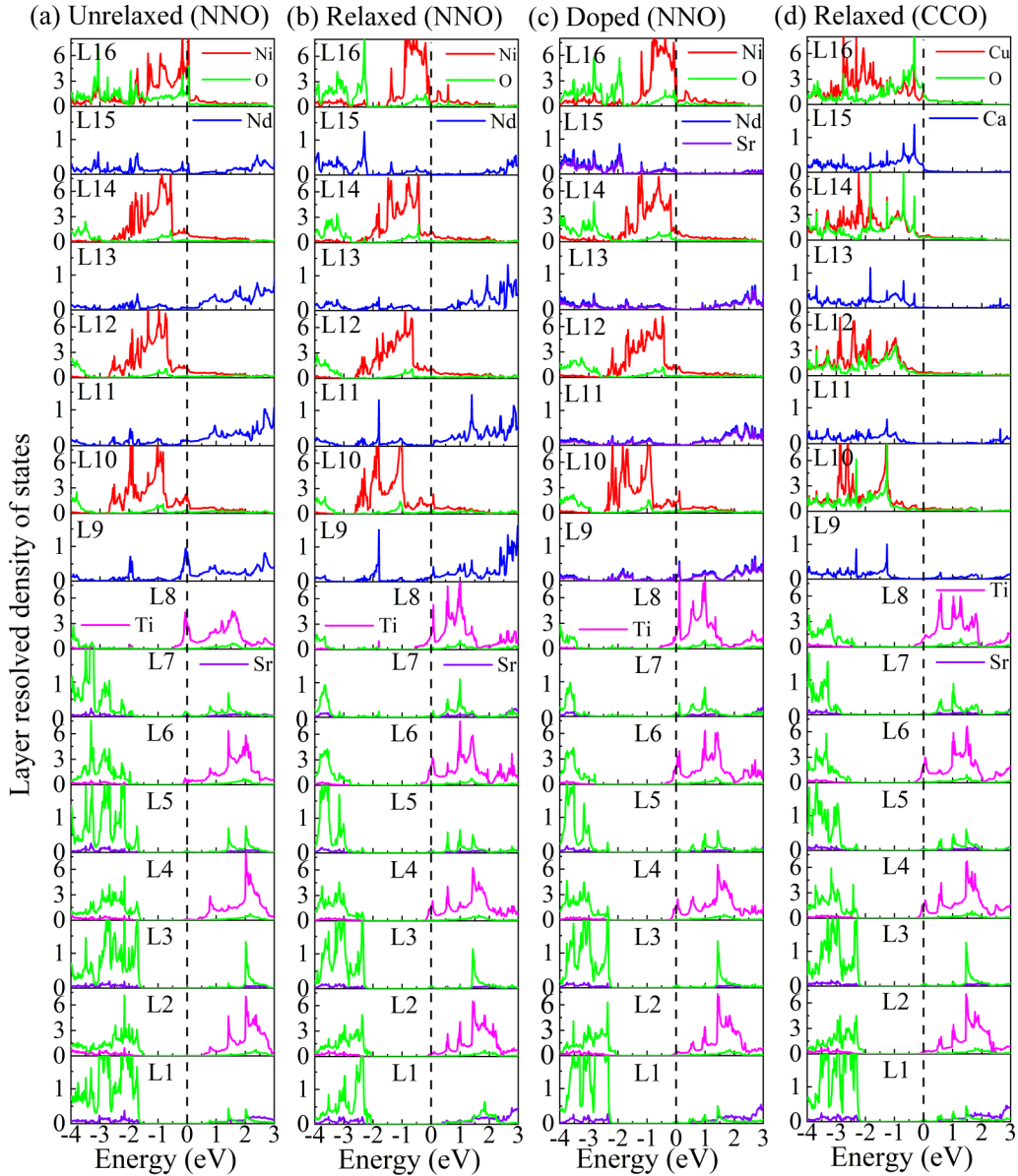
FIG. 3. (a–c) Electronic density of states (DOS) of each layer for the case $(NNO)_4/(STO)_4$, calculated via DFT. The Fermi level is shown with dashed vertical lines. Results presented are for (a) the unrelaxed slab model, (b) the relaxed atomic positions superlattice model, and (c) the 20% hole-doped NNO model. For comparison, we also show (d) the DFT electronic DOS of each layer for the case $(CCO)_4/(STO)_4$ using the relaxed superstructure. The Fermi level is the dashed vertical line.

that a 2DEG emerges at the interface in the NNO films [see Fig. 3(a)].

By introducing the lattice relaxation, the electronic structures of both the interface and surface of NiO_2 are reconstructed and the *p-d* hybridization strength is reduced due to the considerable O-Ni-O bending, in agreement with previous results [38,39], as displayed in Fig. 3(b). Furthermore, this panel indicates that the electrons transfer to the STO substrate. Overall, this suggests that the 2DEG at the interface is caused by the electronic reconstruction due to polar discontinuity. In LAO/STO systems, one possible mechanism relies on the polar catastrophe that plays an important role in the formation of the two-dimensional electron gas, leading to superconductivity [35,35,51]. This suggests that superconductivity in the NNO/STO system of our focus may be related

to an interfacial electron gas as well, as in LAO/STO systems.

To understand the effect of 20% Sr doping in the infinite-layer nickelate, we employed the virtual crystal approximation (VCA) widely used in the electronic structure context [55,56]. As expected, hole doping can be understood using the rigid band picture as shown in Fig. 3(c); namely, the existence of a 2DEG and hole doping at the surface are not qualitatively affected. Based on the analysis of the Ni 3*d* orbital population (not shown), the hole doping at the NiO_2 interface is primarily contributed by the Ni $d_{x^2-y^2}$ orbital. Similarly as in Fig. 3(d), we also observed the electronic reconstruction and strong *p-d* hybridization in the CCO layers. The hole doping at the surface was contributed by the Cu $d_{x^2-y^2}$ orbital, as it occurs for the nickelate.

Furthermore, we also observed that the Ni e_g orbital polarization in the infinite-layer nickelate films, defined as $P = [n(d_{3z^2-r^2}) - n(d_{x^2-y^2})]/[n(d_{3z^2-r^2}) + n(d_{x^2-y^2})]$, increases from interface Ni ($\sim$9%) to surface Ni ($\sim$27%), as in previous results [39]. We also calculated the Ni e_g orbital polarization P for the unrelaxed superstructure and here P increases from interface Ni ($\sim$9.5%) to surface Ni ($\sim$25%), close to the values of the relaxed superstructure. Hence, this e_g orbital polarization is caused by electronic effects, not structural. In addition, we observed that the Cu e_g orbital polarization is smaller than the Ni e_g orbital polarization: P increases from interface Cu ($\sim$7%) to surface Cu ($\sim$15%).

Next, let us discuss the charge transfer at the SrTiO$_3$ interface layers. As shown in Fig. 4 [see Figs. 4(a) and 4(b) compared with bulk, Fig. 4(c) [44]], the Ti d_{xy} orbital starts to be occupied at the interface due to the charge reconstruction caused by the polar discontinuity. This is different from bulk STO where this orbital is unoccupied. More specifically, at the interfacial TiO$_2$ layer, Ti $3d_{xy}$ lowers its energy approximately by -0.58 and -0.37 eV at the Γ point for NNO/STO and CCO/STO interfaces, respectively. This implies that electrons are transferred to the STO substrate from the other component of the superlattice. Since STO is a wideband insulator, not a Mott insulator, the doping by electrons (holes) can be regarded as Fermi level shifts towards the conduction band (valence band). The electronic correlation on the Ti site would not change the charge transfer tendency but can increase the charge transfer values, as in the GGA+U calculations in Ref. [39]. In the previously widely studied case of the LAO/STO interface, also the STO Ti $3d_{xy}$ orbital plays an important role with regard to the interfacial FM and superconductivity, induced by electronic reconstruction [36,37,51,52]. As a consequence, our results indicate that Ti $3d_{xy}$ becomes active at the interface and suggest that this orbital may be important for superconductivity in NNO as well, similarly as in LAO/STO systems. Experimental work is needed to confirm our conjecture but our effort points toward many similarities between LAO/STO and NNO/STO-CCO/STO systems, as well as a nonpassive role of the STO component. In CCO/STO systems, a theory indicates that the introduction of extra oxygen ions at the CCO/STO interface is important for superconductivity [23].

C. Magnetic reconstruction

Theoretical efforts strongly suggest that Néel (G-type) antiferromagnetism (AFM) has the lowest energy on RNiO$_2$ (R = La and Nd) bulk [57–60]. However, magnetization and neutron powder diffraction revealed no long-range magnetic ordering in these compounds, although short-range spin correlations are possible [61,62]. Other explanations have been proposed [20].

To better understand correlation effects and the possible magnetism at the Ni ions, here we use an effective Hubbard coupling ($U_{\text{eff}} = 4$ eV) [39,63] assuming G-AFM magnetic order in the NiO$_2$ layers of the superlattice. It should be noted that the physical description will not change by considering magnetism and electronic correlations on the Ni sites; i.e., the ionic reconstruction, charge transfer, and the strong occupation of the $3d_{xy}$ state are robust conclusions of our effort.
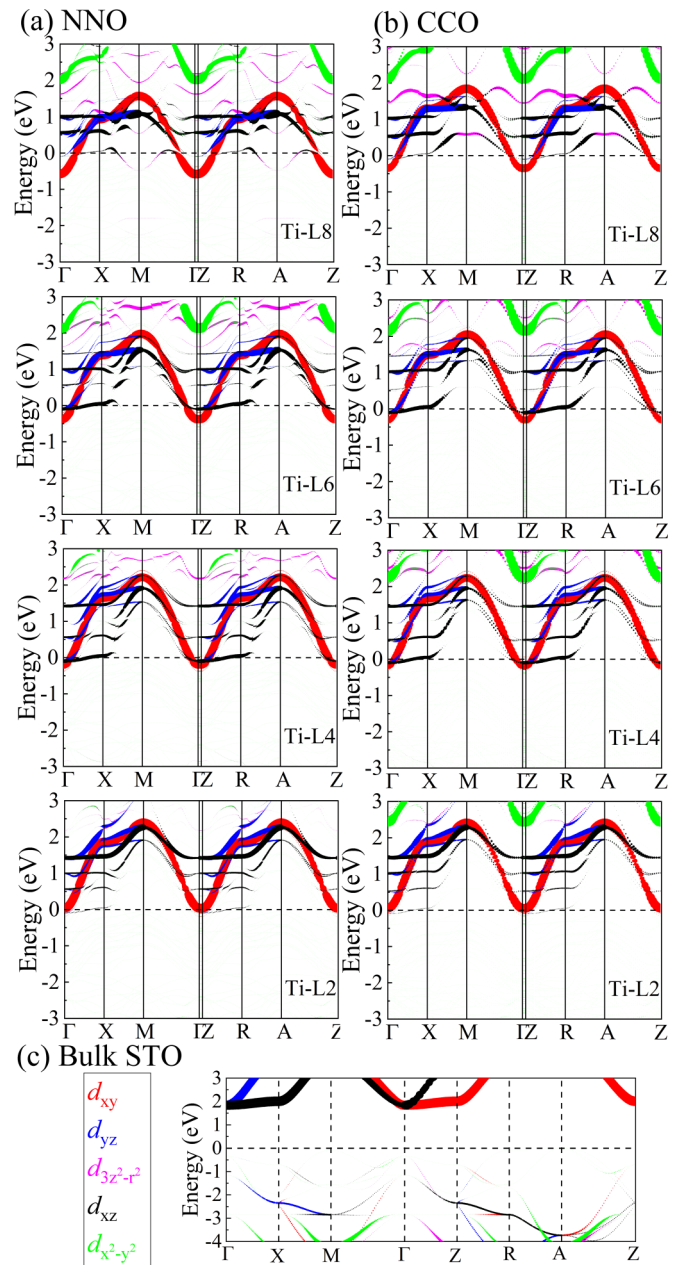

FIG. 4. Projected Ti band structure of the SrTiO$_3$ layers for the nonmagnetic state. The Fermi level is shown with dashed horizontal lines. The weight of each Ti orbital is represented by the thickness of the lines. Note the d_{xy} orbital, particularly at Γ, is starting to be occupied because it is below the Fermi level. The electrons populating this portion of the Ti band arise from the Ni or Cu oxide films which, thus, become hole doped. (a) NNO/STO for various layers [label convention in Fig. 1(a)] and (b) CCO/STO for various layers. For comparison, in (c) we show the Ti bands of STO (bulk form) displaying the typical band-insulator gap and with an unoccupied d_{xy} band, as discussed in the text.

Interestingly, we observed a strong magnetic reconstruction at the NdNiO$_2$ surface layer [see Fig. 5(a)] as compared to the internal layers, such as Fig. 5(d). The surface is basically nonmagnetic. Furthermore, based on our DFT results with G-AFM magnetism and electronic correlation, we estimate
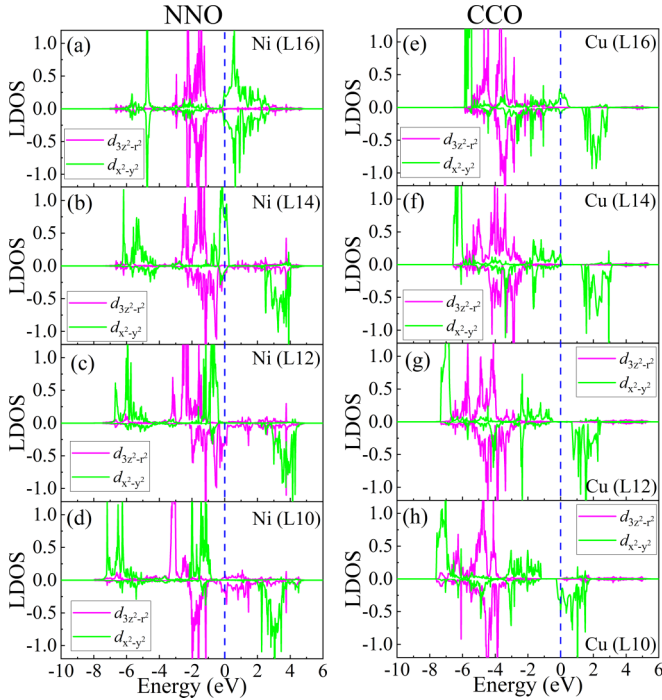
FIG. 5. Ni and Cu projected local DOS corresponding to the e_{2g} orbital of $(NNO)_4/(STO)_4$ and $(CCO)_4/(STO)_4$ assuming a G-AFM-type magnetic configuration. The Fermi level is indicated with dashed lines. Note that we only show the local DOS of one Ni or Cu site at each layer.

that the surface Ni lost approximately $-0.129\ e/\text{Ni}$ while the interface Ti gained about $0.129\ e/\text{Ti}$, as compared with the $3d$ electronic occupation in bulk. Thus, the tendency for charge transfer discussed in Fig. 2(b) was found not to change by introducing the magnetism and electronic correlation.

By studying the DOS in Figs. 5(b)–5(d), we found that the magnetic moments of Ni are primarily contributed by the $d_{x^2-y^2}$ orbital since the electronic occupation of spin up and spin down of $d_{3z^2-r^2}$ are almost equal. In the two NNO layers near STO, $d_{x^2-y^2}$ displays a Mott gap while the $d_{3z^2-r^2}$ orbital remains metallic, which is close to the theoretical results obtained for bulk NNO [64]. As shown in Fig. 5(b), comparing with the L10 and L12 layers, the $3d_{x^2-y^2}$ orbital began to shift across the Fermi level, indicating that the Ni $3d_{x^2-y^2}$ orbital of the L14 layer would also lose some electrons. The hole doping at the surface reduces the electronic occupation of Ni $3d_{x^2-y^2}$, leading the original Ni^{1+} (d^9) to change towards Ni^{2+} (d^8), although there is a partial electronic occupation of $3d_{x^2-y^2}$ [see Figs. 5(a) and 5(d)].

Furthermore, we also considered the case of $U_{\text{eff}} = 6$ eV [65] with the G-AFM magnetic configuration in each CuO_2 layer for the CCO/STO structure. In Fig. 5(e), we calculated that the surface has a moment $0.55\mu_B/\text{Cu}$. The central CuO_2 layers, between surface and interface, still remain insulating while the surface and interfacial CuO_2 layers become metallic due to hole and electron doping, respectively. Different from NNO/STO systems, the Cu $3d_{3z^2-r^2}$ orbital displays doubly occupied behavior and for this reason this orbital is not active for the Cu layers, as widely accepted. In this case, the different

behavior of $d_{3z^2-r^2}$ between nickelate and cuprate films establishes another qualitative difference between the two cases.

IV. CONCLUSIONS

In summary, we systematically studied nickelate and cuprate films grown on an STO substrate by using first-principles calculations. We observed a strong lattice reconstruction in both NNO/STO and CCO/STO systems. In the case of NNO/STO systems, the surface and interfacial NiO_2 layers present opposite displacements, although the net effect still leads to a globally NNO polar film due to different displacement values. For the case of CCO/STO systems, the surface and interfacial CuO_2 layers were distorted in the same direction, again leading to a globally CCO polar film. Moreover, the atomic reconstruction was basically independent of the thickness of the NNO or CCO films, at least up to the eight layers studied here. We also observed a strong electronic reconstruction for the two systems caused by the growing internal electric field (polar catastrophe), as in other superlattices before. In the NNO/STO system, a 2DEG formed at the interfacial layer between NNO and STO, extending over several layers. For the CCO/STO system, on the other hand, the 2DEG was more sharply localized at the interface between CCO and STO. Furthermore, a strong occupation of the Ti $3d_{xy}$ states was observed at the TiO_2 interface for both NNO/STO and CCO/STO systems. In addition, the surface e_g orbital polarization P of Ni was found to be stronger than the surface e_g orbital polarization P of Cu. By introducing magnetism and electronic correlation, the $d_{3z^2-r^2}$ orbital of Ni, which is near insulating in the absence of Hubbard U, remarkably becomes itinerant while the $d_{3z^2-r^2}$ orbital of Cu remains doubly occupied. For this reason, we believe that the NNO grown on STO requires a two-orbital description as often employed in nickelates, while CCO admits the canonical one-orbital formulation standard for cuprates. In addition, we also observed a strong magnetic reconstruction at the $NdNiO_2$ surface to vacuum layer where magnetism is basically suppressed.

APPENDIX A: ELECTRONIC STRUCTURE OF BULK $NdNiO_2$ AND $CaCuO_2$

$NdNiO_2$ forms a $P4/nmm$ tetragonal crystal structure, similar to $CaCuO_2$ [see Fig. 6(a)]. As shown in Figs. 6(b) and 6(c), the electronic density near the Fermi level is mainly contributed by the Cu or Ni atoms. The main difference is that there is a strong p-d hybridization in $CaCuO_2$ but this hybridization is quite weak in $NdNiO_2$ (the latter is contrary
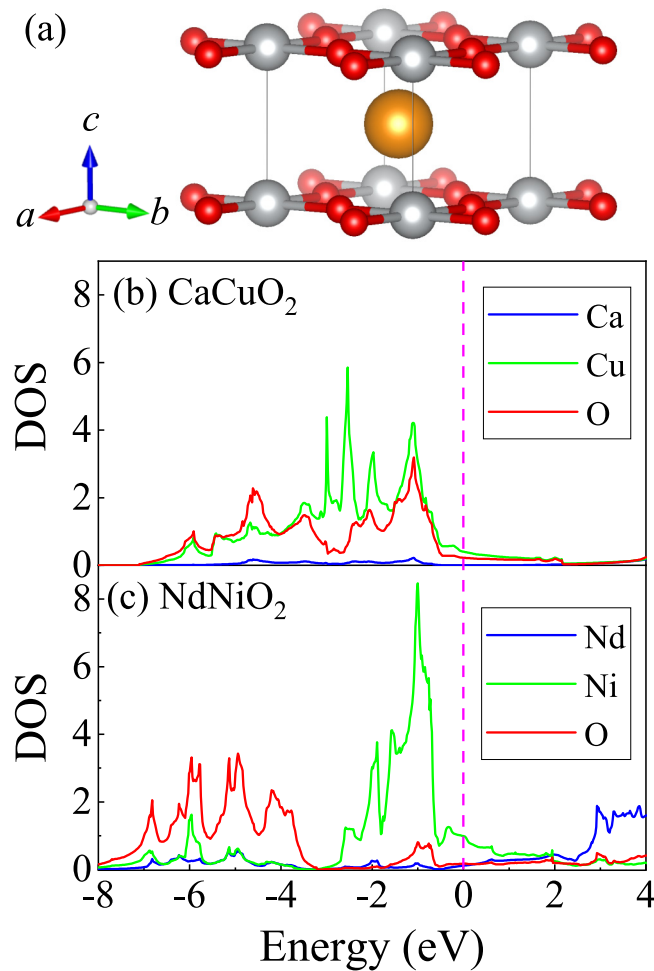
FIG. 6. (a) Schematic crystal structure of ABO_2 (electronic density $n = 9$) with the following convention: orange, Sr or Nd; gray, Cu or Ni; and red, O. DOS near the Fermi level using the nonmagnetic states for (b) CaCuO$_2$ and (c) NdNiO$_2$.

to the results for NNO/STO shown in the main text where the p-d hybridization is larger). In the case of Cu, only one Cu $d_{x^2-y^2}$ band crosses the Fermi energy. However, there are two bands crossing the Fermi level for nickelates, Ni $d_{x^2-y^2}$ and Nd $d_{3z^2-r^2}$, the latter hybridized with d_{yz}, as displayed in Fig. 7(a) and 7(b). The $3d_{x^2-y^2}$ orbital is more dispersive along the xy plane than along the z direction due to the Cu-O or Ni-O antibonding character. The O $2p$ bands of NdNiO$_2$ extend over a broad range of energy from -10 to 2 eV indicating that the charge transfer energy is quite larger than for CaCuO$_2$. Another interesting result is that the $3d_{3z^2-r^2}$ orbital of Ni is more broad than the $3d_{3z^2-r^2}$ orbital of Cu. This implies that the $3d_{3z^2-r^2}$ orbital of Ni may display different behavior as the same orbital in Cu. Based on the Wannier fitting using the WANNIER90 packages [66], we estimate the charge transfer energy $\Delta = \varepsilon_d - \varepsilon_O$ to be 1.7 eV for CaCuO$_2$ and 4.2 eV for NdNiO$_2$.

APPENDIX B: COMPRESSIVE STRAIN ON THE EPITAXIAL CONSTRAINT TO STO

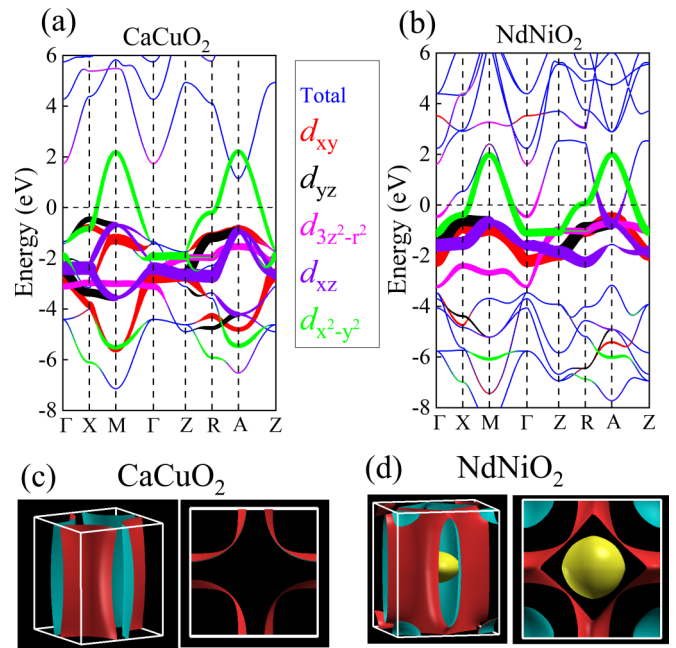Our relaxed crystal lattice constants of cubic STO are $a = b = c = 3.943$ Å. If we fix two of them as

FIG. 7. Projected band structures of (a) CaCuO$_2$ and (b) NdNiO$_2$ for the nonmagnetic state. The Fermi level is shown with horizontal dashed lines. The weight of each orbital is represented by the thickness of the lines. Fermi surface of (c) CaCuO$_2$ and (d) NdNiO$_2$.

$a = b = 3.943$ Å without polar distortion, then the relaxed lattice constant of the c axis becomes 4.032 Å and the strained STO is still paraelectric. However, if we introduce a polar distortion along the c axis in a fixed structure, the energy becomes lower than the strained STO without polar distortion. In
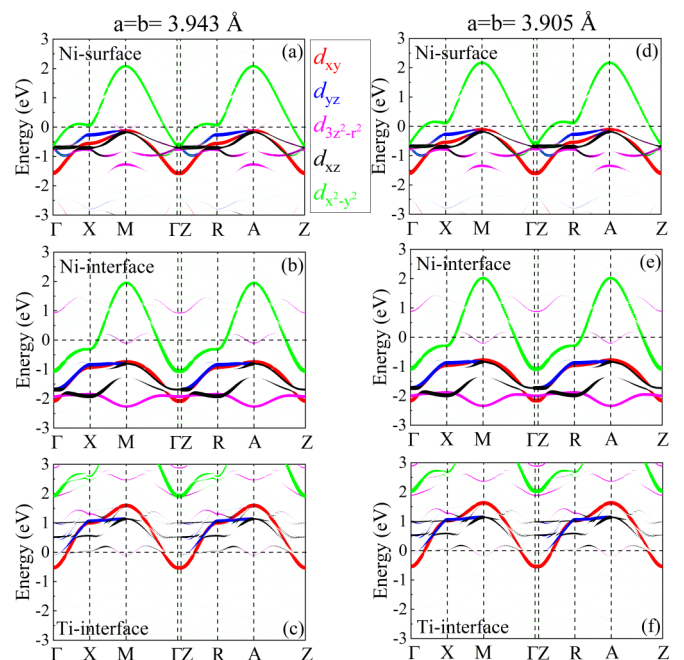

FIG. 8. Projected band structures of Ni and interface Ti for the case (NNO)$_2$/(STO)$_4$ using $a = b = 3.905$ Å and $a = b = 3.943$ Å, respectively. The Fermi level is shown with horizontal dashed lines. The weight of each orbital is represented by the thickness of the lines.
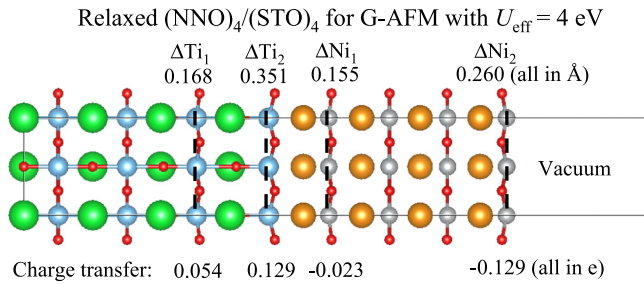
Relaxed $(NNO)_4/(STO)_4$ for G-AFM with $U_{eff} = 4$ eV

FIG. 9. Schematic relaxed slab model of $(NNO)_n/(STO)_4$ for G-AFM order ($U_{eff} = 4$ eV) with the following convention: orange, Nd or Ca; gray, Ni or Cu; red, O; green, Sr; and blue, Ti. Here, we fixed $a = b = 3.905$ Å. We considered two undistorted STO layers (namely, with atomic positions fixed) to simulate the effects of the rest of the STO substrate.

this case, the system then changes to a ferroelectric tetragonal phase. Since the optimized in-plane lattices of STO ($a = b = 3.943$ Å) are slightly larger than the experimental values (3.905 Å), it would generate a moderate compressive strain. To better understand this point, we also calculated the two-layer $NdNiO_2$ slab model by fixing the in-plane lattice to the optimized STO ($a = b = 3.943$ Å). After a full structural optimization relaxation, the bending behavior of the NiO_2 layers do not change. The corresponding Ni ions still move towards *different* directions with displacements $\Delta = 0.279$ and -0.169 Å, quite close to the results of $n = 2$ NNO/STO with fixed experimental in-plane lattice constants ($\Delta = 0.291$ and -0.184 Å). Furthermore, the interfacial Ti ions of the STO substrate still show ferroelectric-like displacements away from the NNO/STO interface with values $\Delta = -0.291$ and -0.145 Å, respectively, which is in closer agreement with the distortions of Ti for a fixed $a = b = 3.943$ Å ($\Delta = -0.301$ and -0.157 Å). In addition, the hole doping at the interface, charge transfer behavior, existence of a 2DEG, electronic occupation of the Ti $3d_{xy}$ orbital, and other physical properties are consistent with the NNO/STO ($n = 2$) slab using fixed

experimental STO lattice constants. For the benefit of the readers, we compared the band structures of Ni, at surface and interface, and interface Ti for the two cases, as shown in Fig. 8.

APPENDIX C: CHARGE TRANSFER WITH U_{eff}

To better understand the charge transfer, we performed DFT+U_{eff} calculations using a $(NNO)_4/(STO)_4$ slab. On one hand, we fully relaxed the structure with the G-AFM configuration by using $U_{eff} = 4$ eV on Ni sites, since both electronic and atomic structure will affect the charge transfer. As shown in Fig. 9, both the surface and interfacial Ni ions move in *different* directions, with displacements $\Delta = 0.260$ and -0.155 Å, which is slightly reduced by comparing with results of DFT for the NM state ($\Delta = 0.296$ and -0.189 Å). Based on our calculations, from surface to interface, the lost electrons at each Ni are -0.129, -0.031, -0.001, and -0.023 e/Ni, respectively, while the Ti_1 and Ti_2 captured electrons are about 0.054 and 0.129 e/Ti. In contrast, the results of DFT of NM are -0.101, -0.023, -0.005, and -0.012 e/Ni, respectively.

On the other hand, we also added $U_{eff} = 4$ eV directly to the optimized structure from pure GGA (namely, keeping the atomic distortions unchanged) since the atomic structure only slightly changed in the DFT+U_{eff} calculations. In this case, we estimate that the surface Ni lost approximately -0.141 e/Ni while the interface Ti gained about 0.126 e/Ti, as shown in Table I. Hence, the charge transfer is enhanced by introducing U_{eff}.

TABLE I. The charge transfer of Ni and Ti atoms for different $U_{eff} = 4$ eV based on the optimized GGA structure, compared with the corresponding bulk values. The subscript "int" ("sur") denotes interface (surface).

	Ti_1	Ti_2	Ni_{int}	Ni_{sur}
Without U_{eff}	0.065	0.114	-0.012	-0.101
$U_{eff} = 4$ eV	0.06	0.114	-0.009	-0.141

[1] J. G. Bednorz and K. A. Müller, Z. Phys. B: Condens. Matter **64**, 189 (1986).

[2] E. Dagotto, Rev. Mod. Phys. **66**, 763 (1994).

[3] G. R. Stewart, Rev. Mod. Phys. **83**, 1589 (2011).

[4] D. J. Scalapino, Rev. Mod. Phys. **84**, 1383 (2012).

[5] E. Dagotto, Rev. Mod. Phys. **85**, 849 (2013).

[6] D. Li, K. Lee, B. Y. Wang, M. Osada, S. Crossley, H. R. Lee, Y. Cui, Y. Hikita, and H. Y. Hwang, Nature **572**, 624 (2019).

[7] Y. Nomura, M. Hirayama, T. Tadano, Y. Yoshimoto, K. Nakamura, and R. Arita, Phys. Rev. B **100**, 205138 (2019).

[8] A. S. Botana and M. R. Norman, Phys. Rev. X **10**, 011024 (2020).

[9] D. Li, B. Y. Wang, K. Lee, S. P. Harvey, M. Osada, B. H. Goodge, L. F. Kourkoutis, and H. Y. Hwang, Phys. Rev. Lett. **125**, 027001 (2020).

[10] M. Hepting, D. Li, C. J. Jia, H. Lu, E. Paris, Y. Tseng, X. Feng, M. Osada, E. Been, Y. Hikita, Y.-D. Chuang, Z. Hussain, K. J. Zhou, A. Nag, M. Garcia-Fernandez, M. Rossi, H. Y. Huang, D. J. Huang, Z. X. Shen, T. Schmitt, H. Y. Hwang, B. Moritz, J. Zaanen, T. P. Devereaux, and W. S. Lee, Nat. Mater. **19**, 381 (2020).

[11] M. Azuma, Z. Hiroi, M. Takano, Y. Bando, and Y. Takeda, Nature **356**, 775 (1992).

[12] H. Sakakibara, H. Usui, K. Suzuki, T. Kotani, H. Aoki, and K. Kuroki, Phys. Rev. Lett. **125**, 077003 (2020).

[13] M. Jiang, M. Berciu, and G. A. Sawatzky, Phys. Rev. Lett. **124**, 207004 (2020).

[14] X. Wu, D. DiSante, T. Schwemmer, W. Hanke, H. Y. Hwang, S. Raghu, and R. Thomale, Phys. Rev. B **101**, 060504(R) (2020).

[15] G.-M. Zhang, Y.-F. Yang, and F.-C. Zhang, Phys. Rev. B **101**, 020501(R) (2020).

[16] P. Werner and S. Hoshino, Phys. Rev. B **101**, 041104(R) (2020).

[17] Y. Gu, S. Zhu, X. Wang, J. Hu, and H. Chen, Commun. Phys. **3**, 84 (2020).

[18] J. Karp, A. S. Botana, M. R. Norman, H. Park, M. Zingl, and A. Millis, Phys. Rev. X **10**, 021061 (2020).

[19] M. Kitatani, L. Si, O. Janson, R. Arita, Z. Zhong, and K. Held, npj Quantum Mater. **5**, 59 (2020).

[20] Q. Li, C. He, J. Si, X. Zhu, Y. Zhang, and H.-H. Wen, Commun. Mater. **1**, 16 (2020).

[21] B.-X. Wang, H. Zheng, E. Krivyakina, O. Chmaissem, P. P. Lopes, J.-W. Lynn, L. C. Gallington, Y. Ren, S. Rosenkranz, J. F. Mitchell, and D. Phelan, Phys. Rev. Mater. **4**, 084409 (2020).

[22] C. Aruta, C. Schlueter, T.-L. Lee, D. Di Castro, D. Innocenti, A. Tebano, J. Zegenhagen, and G. Balestrino, Phys. Rev. B **87**, 155145 (2013).

[23] D. Di Castro, C. Cantoni, F. Ridolfi, C. Aruta, A. Tebano, N. Yang, and G. Balestrino, Phys. Rev. Lett. **115**, 147001 (2015).

[24] S. Thiel, G. Hammerl, A. Schmehl, C. W. Schneider, and J. Mannhart, Science **313**, 1942 (2006).

[25] N. Reyren, S. Thiel, A. D. Caviglia, L. F. Kourkoutis, G. Hammerl, C. Richter, C. W. Schneider, T. Kopp, A.-S. Rüetschi, D. Jaccard, M. Gabay, D. A. Muller, J.-M. Triscone, and J. Mannhart, Science **317**, 1196 (2007).

[26] E. Dagotto, Nature **469**, 167 (2011).

[27] S. Piskunov and R. I. Eglitis, Solid State Ionics **274**, 29 (2015).

[28] S. Piskunov, R. I. Eglitis, and Y. F. Zhukovskii, Phys. Status Solidi C **13**, 913 (2016).

[29] H. Chen, D. P. Kumah, A. S. Disa, F. J. Walker, C. H. Ahn, and S. Ismail-Beigi, Phys. Rev. Lett. **110**, 186402 (2013).

[30] H. Chen, A. J. Millis, and C. A. Marianetti, Phys. Rev. Lett. **111**, 116403 (2013).

[31] A. S. Disa, D. P. Kumah, A. Malashevich, H. Chen, D. A. Arena, E. D. Specht, S. Ismail-Beigi, F. J. Walker, and C. H. Ahn, Phys. Rev. Lett. **114**, 026801 (2015).

[32] A. Ohtomo, D. A. Muller, J. L. Grazul, and H. Y. Hwang, Nature **419**, 378 (2002).

[33] A. Ohtomo and H. Y. Hwang, Nature **427**, 423 (2004).

[34] A. Brinkman, M. Huijben, M. van Zalk, J. Huijben, U. Zeitler, J. C. Maan, W. G. van der Wiel, G. Rijnders, D. H. A. Blank, and H. Hilgenkamp, Nat. Mater. **6**, 493 (2007).

[35] N. Nakagawa, H. Y. Hwang, and D. A. Muller, Nat. Mater. **5**, 204 (2006).

[36] D. A. Dikin, M. Mehta, C. W. Bark, C. M. Folkman, C. B. Eom, and V. Chandrasekhar, Phys. Rev. Lett. **107**, 056802 (2011).

[37] N. Pavlenko, T. Kopp, E. Y. Tsymbal, G. A. Sawatzky, and J. Mannhart, Phys. Rev. B **85**, 020407(R) (2012).

[38] R. He, P. Jiang, Y. Lu, Y. Song, M. Chen, M. Jin, L. Shui, and Z. Zhong, Phys. Rev. B **102**, 035118 (2020).

[39] B. Geisler and R. Pentcheva, Phys. Rev. B **102**, 020502(R) (2020).

[40] G. Kresse and J. Hafner, Phys. Rev. B **47**, 558(R) (1993).

[41] G. Kresse and J. Furthmüller, Phys. Rev. B **54**, 11169 (1996).

[42] P. E. Blöchl, Phys. Rev. B **50**, 17953 (1994).

[43] J. P. Perdew, K. Burke, and M. Ernzerhof, Phys. Rev. Lett. **77**, 3865 (1996).

[44] The band gap of STO is 1.86 eV based on GGA calculations. This value is smaller than the experimental value (∼3.2 eV)

[34], since the DFT technique usually underestimates the band gap of ABO_3 perovskite materials. It should be noted that hybrid-exchange correlation functionals, such as B3LYP, allow to achieve an excellent agreement with experiments for the band gaps of related ABO_3 perovskites, their (001) surfaces, and heterostructures [45]. The hybrid-exchange correlation functional provides only a correction for the band gap, and does not change other physical properties. However, the scope of this publication is to focus on the physical properties at the interface.

[45] R. I. Eglitis and A. I. Popov, J. Saudi Chem. Soc. **22**, 459 (2018).

[46] T. Mitsui *et al.*, in *Ferroelectrics and Related Substances: Oxides*, edited by K.-H. Hellwege and O. Madelung, Landolt-Börnstein, Group III Condensed Matter Vol. 16, Part A (Springer-Verlag, Berlin, 1981).

[47] R. Pentcheva and W. E. Pickett, Phys. Rev. Lett. **102**, 107602 (2009).

[48] Here, the charge transfer was calculated by comparing the difference of occupied number of $3d$ orbitals between superlattice and corresponding bulk structure.

[49] H. Chen and A. Millis, J. Phys.: Condens. Matter **29**, 243001 (2017).

[50] Z. Zhong and P. Hansmann, Phys. Rev. X **7**, 011023 (2017).

[51] S. Okamoto and A. J. Millis, Nature **428**, 630 (2004).

[52] J. A. Bert, B. Kalisky, C. Bell, M. Kim, Y Hikita, H. Y. Hwang, and K. A. Moler, Nat. Phys. **7**, 767 (2011).

[53] Since we verified that the film thickness of NNO or CCO does not change the main physical conclusions of our work, we primarily discussed our main results using the $(NNO)_4/(STO)_4$ or $(CCO)_4/(STO)_4$ heterostructures, corresponding to a film thickness of four unit cells.

[54] A. Savin, O. Jepsen, J. Flad, O.-K. Andersen, H. Preuss, and H. G. von Schnering, Angew. Chem. Int. Ed. **31**, 187 (1992).

[55] L. Bellaiche and D. Vanderbilt, Phys. Rev. B **61**, 7877 (2000).

[56] N. J. Ramer and A. M. Rappe, Phys. Rev. B **62**, R743(R) (2000).

[57] K.-W. Lee and W. E. Pickett, Phys. Rev. B **70**, 165109 (2004).

[58] S. Ryee, H. Yoon, T. J. Kim, M. Y. Jeong, and M. J. Han, Phys. Rev. B **101**, 064513 (2020).

[59] H. Zhang, L. Jin, S. Wang, B. Xi, X. Shi, F. Ye, and J.-W. Mei, Phys. Rev. Research **2**, 013214 (2020).

[60] I. Leonov and S. Y. Savrasov, arXiv:2006.05295v2.

[61] M. A. Hayward and M. J. Rosseinsky, J. Am. Chem. Soc. **121**, 8843 (1999).

[62] M. A. Hayward and M. J. Rosseinsky, Solid State Sci. **5**, 839 (2003).

[63] S. L. Dudarev, G. A. Botton, S. Y. Savrasov, C. J. Humphreys, and A. P. Sutton, Phys. Rev. B **57**, 1505 (1998).

[64] F. Lechermann, Phys. Rev. B **101**, 081110(R) (2020).

[65] H. J. Xiang, C. Lee, and M.-H. Whangbo, Phys. Rev. B **76**, 220411(R) (2007).

[66] A. A. Mostofi, J. R. Yates, Y. S. Lee, I. Souza, D. Vanderbilt, and N. Marzari, Comput. Phys. Commun. **178**, 685 (2007).